



## Auroral signatures of the plasma injection and dipolarization in the inner magnetosphere

V. A. Sergeev,<sup>1</sup> T. A. Kornilova,<sup>2</sup> I. A. Kornilov,<sup>2</sup> V. Angelopoulos,<sup>3</sup> M. V. Kubyshkina,<sup>1</sup> M. Fillingim,<sup>4</sup> R. Nakamura,<sup>5</sup> J. P. McFadden,<sup>4</sup> and D. Larson<sup>4</sup>

Received 2 June 2009; revised 20 August 2009; accepted 16 September 2009; published 3 February 2010.

[1] Using auroral TV data and particle precipitation data from low-altitude satellites, we identify the ionospheric signature of magnetotail dipolarizations and substorm injections measured in the near-Earth near-equatorial plasma sheet by Time History of Events and Macroscale Interactions during Substorms (THEMIS). Field line mapping exploits a recently developed time-dependent adaptive model which minimizes the variance to THEMIS in situ magnetotail observations. We present strong evidence that the equatorward edge of the auroral bulge corresponds to the innermost extent of earthward propagating dipolarization fronts in the magnetosphere, whereas individual equatorward moving auroral enhancements correspond to the motion of individual injection fronts reaching at times distances as close to Earth as  $5.5 R_E$ . The region of tail dipolarization corresponds to the auroral bulge, a broad spatial region of enhanced but structured auroral emissions, bounded on the poleward side by discrete auroral forms and on the equatorward side by a sharp drop in auroral luminosity and particle precipitation. Particle precipitation within the bulge is enhanced considerably at the energies above 30 keV. Ionospheric protons are isotropic and electrons are anisotropic but with fluctuating fluxes which are below, but on occasion comparable with, trapped levels. The equatorward edge of the bulge, herein termed the “Equatorward edge of Auroral Bulge” propagates during substorm expansion toward lower latitudes, initially fast (corresponding to 100 km/s in space at  $r \sim 7 R_E$ ) but with decreasing speed after onset. Our adaptive model mapping suggests that equatorial points at near-geosynchronous altitude can map to ionospheric magnetic latitudes up to  $2^\circ$ – $3^\circ$  off of predictions using standard T96 models. The offsets can be either toward lower latitudes due to field line stretching before auroral breakup or toward higher latitudes after breakup due to the near-Earth tail dipolarization.

**Citation:** Sergeev, V. A., T. A. Kornilova, I. A. Kornilov, V. Angelopoulos, M. V. Kubyshkina, M. Fillingim, R. Nakamura, J. P. McFadden, and D. Larson (2010), Auroral signatures of the plasma injection and dipolarization in the inner magnetosphere, *J. Geophys. Res.*, 115, A02202, doi:10.1029/2009JA014522.

### 1. Introduction

[2] Auroral observations were the starting point of substorm research, introduced by Akasofu and Chapman [Akasofu, 1964]. A large amount of observational and theoretical knowledge has resulted since then in the paradigm of a “magnetospheric substorm” as the dominant global energy transformation process in Earth’s magnetosphere [Akasofu, 1977]. Auroral dynamics, being one of the consequences

of magnetospheric dynamics but encompassing its own unique processes (such as particle precipitation, field-aligned particle acceleration, small-scale intense Alfvén wave acceleration) superimposed onto the driving mechanism of magnetospheric dynamics, still play a special role in the investigation of substorms as the ionosphere represents the only present possibility to observe both the global dynamical picture of a magnetospheric substorm and its fine details.

[3] Substorm dipolarization and plasma injections are major disturbances of the inner magnetosphere concurrent with substorm expansion. They are thought to represent an inward motion of plasma, produced by either near-Earth reconnection or current disruption. They are essential components of the magnetic reconfiguration and plasma acceleration occurring at or after substorm onset. Azimuthal progression of the substorm dipolarization is often synonymous with the expansion of the substorm current wedge (SCW) current system in local time. Being historically old concepts [e.g., Russell and McPherron, 1973; McIlwain, 1974], dipolariza-

<sup>1</sup>Institute of Physics, St. Petersburg State University, Saint Petersburg, Russia.

<sup>2</sup>Polar Geophysical Institute, Apatity, Russia.

<sup>3</sup>Institute of Geophysics and Planetary Physics, University of California, Los Angeles, California, USA.

<sup>4</sup>Space Science Laboratory, University of California, Berkeley, California, USA.

<sup>5</sup>Space Research Institute, Austrian Academy of Sciences, Graz, Austria.

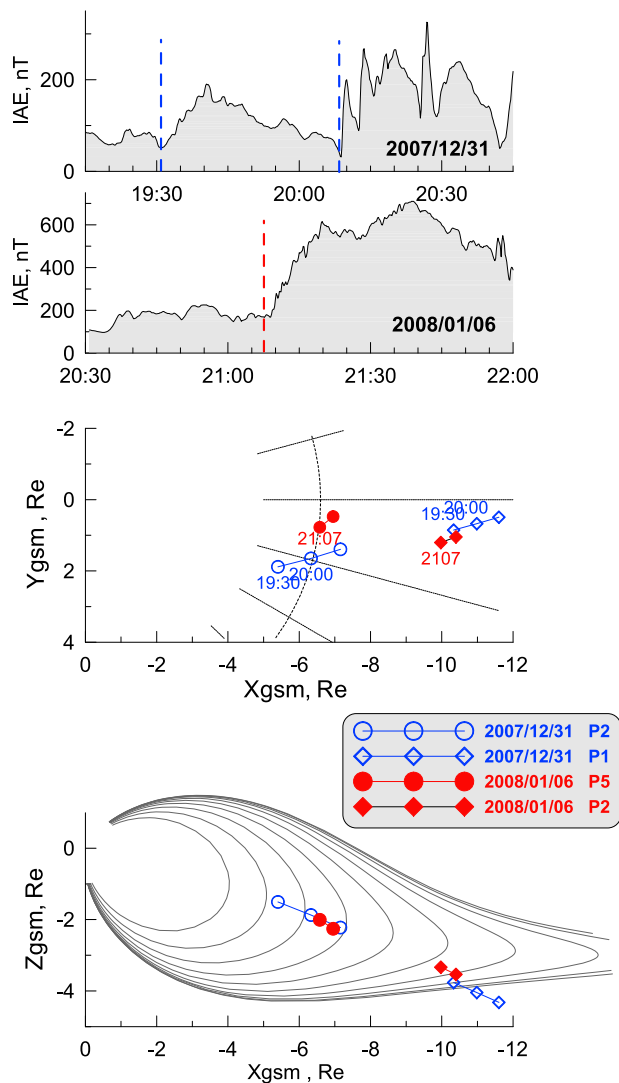


**Figure 1.** (top) International Monitor for Auroral Geomagnetic Effects magnetometer network-based AE index for two substorms. (bottom) Trajectories of pairs of THEMIS probes during two substorm events.

tions, SCW and injections are so familiar from reviews and textbooks that they are often accepted as well-established descriptions of these processes despite the fact that for individual cases, especially involving multiple satellites, this picture can be an oversimplified abstraction, valid only in an average sense and over a large timescale. Among the complications that riddle individual studies today is that according to observations made between 6.6 and about 10  $R_E$  distances [e.g., Ohtani, 1998], the dipolarization contains magnetic fluctuations but at the same time often displays a sharp inner edge which propagates earthward at comparatively low speeds (a few hundreds of km/s). On rare occasions, particle injections at the inner edge have also been observed by radially separated spacecraft [Reeves *et al.*, 1996; Apatenkov *et al.*, 2007] at the aforementioned speed. The information concerning the final stage of this intrusion is scarce, so the braking of the plasma injection is one of the major under-sampled processes and its physics of interaction with the dipolar field and its dissipation

represents one of the major questions in magnetotail physics today.

[4] The starting point of any magnetospheric substorm scenario is the localized auroral breakup which exhibits significant poleward expansion and demarcates the onset of the substorm expansion phase. Its time and location reveal (with appropriate time delays and to within significant mapping uncertainties) the time and location of explosive dissipation in the tail plasma sheet, and the following auroral dynamics reflects, particularly, changes in intensity, location, and amount of reconnected flux in the tail. The poleward bright arc may be an ionospheric projection of the reconnection separatrix and the velocity of poleward expansion provides a measure of the reconnected magnetic flux rate, with reconnected tubes containing newly accelerated plasma. The proportionality between the magnetic flux stored in the lobe before substorm onset and the magnetic flux delineated by the auroral bulge on global images as well as their consistent mapping has been experimentally confirmed [Shukhtina *et al.*, 2005; Yahnin *et al.*, 2006].

[5] The poleward surging discrete auroras develop into a bulge which they also envelop. Within the bulge, the area of intense precipitation equatorward of the advancing auroras, the auroral structures are quite dynamic, often structured (filamented and patchy), and on occasion exhibiting north-south arcs and equatorward moving arcs [Nakamura *et al.*, 1993]. On the equatorward side, the region of enhanced precipitation may terminate without any distinct arc delineating its border. We will refer to this border as the Equatorward edge of the Auroral Bulge, or EAB, and we will see that it is not necessarily collocated with the inner edge of the plasma sheet. Unlike the active poleward auroras which have been in the focus of auroral research, the auroral activity inside the auroral bulge and near its equatorward edge has usually been neglected in previous studies.

[6] In this paper we investigate two substorm events with favorable coverage of both auroral and spacecraft observations in order to address the auroral morphology and dynamics on the field lines in the inner magnetosphere, where the dipolarization and plasma injections are simultaneously observed by Time History of Events and Macroscale Interactions during Substorms (THEMIS). Using auroral TV measurements we address the dynamics and morphology of the EAB. Using NOAA-POES observations, we describe the auroral and energetic particle precipitation in the equatorward part of auroral bulge. Using advanced magnetic field models, we map between the ionosphere and magnetic equator in order to address the relationship between the EAB and the dipolarization and plasma injection in the equatorial magnetosphere.

## 2. Observations

### 2.1. General

[7] The auroral observations presented herein include global imaging by Polar UVI instrument in the Lyman-Birge-Hopfield long filter (LBHL) band at 36 s time resolution [Torr *et al.*, 1995] in the Southern Hemisphere as well as ground TV observations at closely spaced observatories Loparskaya (LOP, 68.63°N, 33.25°E) and Lovozero (LOZ, 67.97°N, 35.02°E), with magnetic midnight at about 21.7 h UT. Details of the TV recordings and data processing

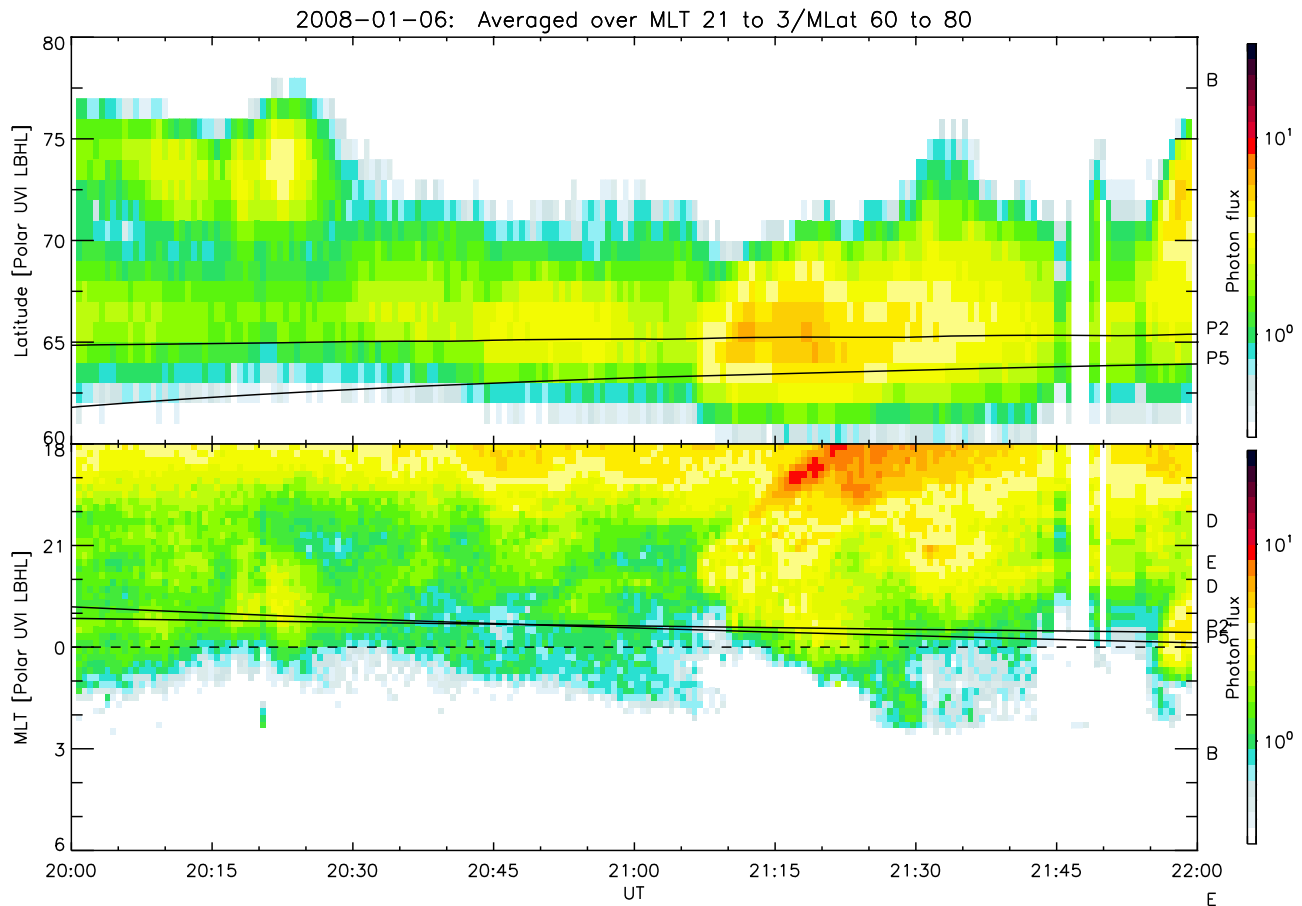


**Figure 2.** Polar UVI LBHL-band global images (top) in keogram CGLat-UT format (averaged over MLT in  $\pm 3$  h MLT sector near midnight) and (bottom) in MLT-UT format (averaged over meridians between  $60^\circ$  and  $75^\circ$  CGLat). Black lines show the trajectories of THEMIS probes P2 and P5 mapped to the ionosphere.

have been given by *Kornilova et al.* [2008]. Precipitated and trapped fluxes of auroral particles (0.3–20 keV, Total Energy Detector (TED) instrument) and energetic particles (at  $>30$  and  $>100$  keV energies, Medium Energy Proton and Electron Detector (MEPED) instrument) were measured by the polar orbiting, low-altitude ( $h \sim 850$  km) NOAA-POES spacecraft (see *Evans and Greer* [2006] for a description of the instruments and data formats). The THEMIS mission is a five-satellite constellation in the equatorial magnetosphere [see *Angelopoulos*, 2008, and references therein]. In this paper we use spin-resolution observations from the fluxgate magnetometer (FGM) and particle instruments (electrostatic analyzer (ESA) and solid state telescope (SST)) on two of the THEMIS spacecraft (probes) in the outbound leg of their orbits through the inner magnetosphere near the midnight meridian (Figure 1). The inner and outer spacecraft were probes P5 and P2 in the case of a strong substorm on 6 January 2008, whereas they were probes P2 and P1 on 31 December 2007. During both events, around substorm onset the innermost probes were positioned close to the magnetic equator near the geostationary distance. The outermost spacecraft were only  $1\text{--}2 R_E$  below the neutral sheet, at about  $11 R_E$  distance, yet they observed the plasma sheet boundary and even temporarily exited to the lobe, indicating that the current sheet was thin at the time. Whereas the innermost spacecraft are

the main source of information concerning the timing of dipolarization and injection in the inner magnetosphere, both spacecraft (together with the remaining three THEMIS probes) provide valuable data for adapting the magnetospheric model used in our study for our mapping, an essential aspect of our study. Our modeling effort proceeds as follows. First, we used the standard T96 model with input taken from propagated 5-min-averaged solar wind data from the OMNI data set. Next, we use the simplest adaptive model (AM-01) of *Kubyshkina et al.* [2009] which relies on T96 model formulas, but with coefficients obtained by fitting the model at any particular time to the magnetic observations made by the five THEMIS probes. Comparisons between the two models (standard and adaptive) and between model-predicted and observed magnetic fields in the region of interest (at THEMIS) allow us to further evaluate and control the effects and quality of mapping.

## 2.2. Auroral and Particle Observations

[8] The substorm on 6 January 2008 had a major onset at about 2107 UT, after which the Image AE index quickly rose to about 600 nT in about 20 min (Figure 1). The substorm was also seen in the 36 s resolution Polar UVI data, as evident by the start of auroral brightening in the pre-midnight sector at 2107:01 UT in Figure 2. The ionospheric

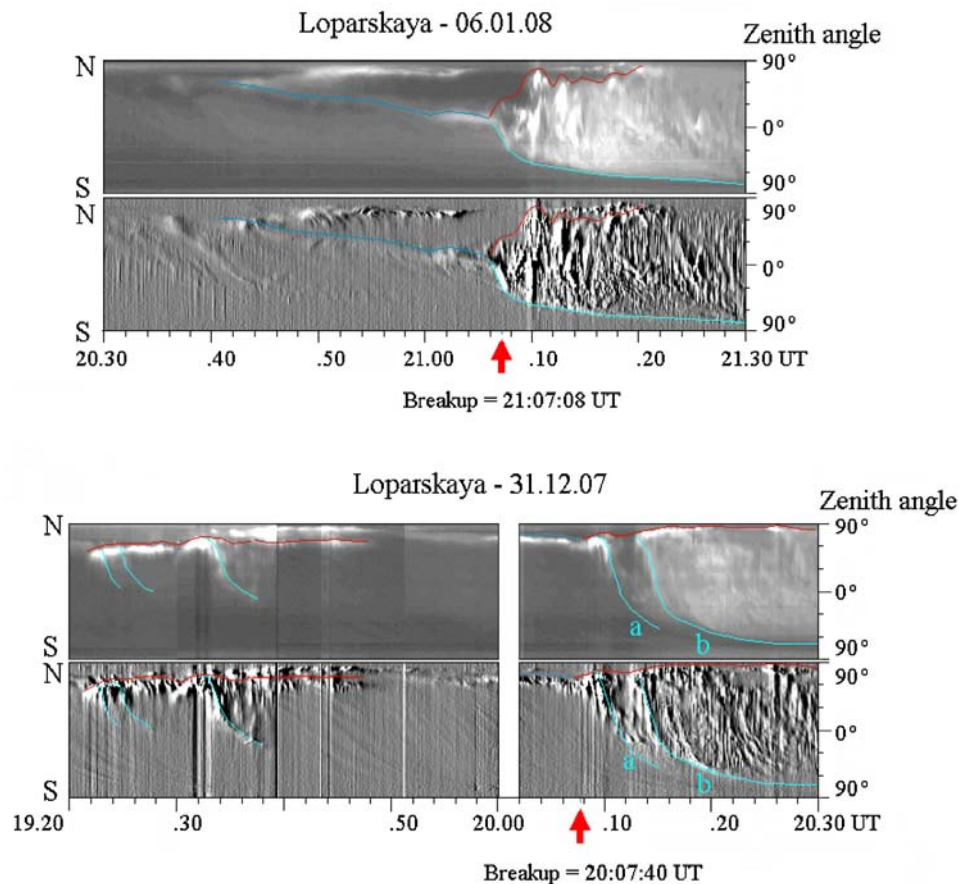


**Figure 3.** (top) TV keograms for the 6 January 2008 substorm from LOP. Both total brightness and differential brightness keograms are presented (top and bottom keograms, respectively), the breakup time is shown by an arrow, and the poleward border of bright active auroras and the equatorward-moving auroral enhancement traces forming together the equatorward border of auroral bulge are marked by red and blue lines. (bottom) The same but for the 31 December 2007 substorm.

footprints of THEMIS probes P2 and P1 are demarcated by the two solid lines through the UVI spectrogram. The two TV cameras at LOZ and LOP were located at 23.4 h magnetic local time (MLT) at this time, i.e., at the dawnside of the brightening region and near the meridian of the two Themis probes P2 and P1.

[9] Keograms (Figure 3, two top parts) and all-sky snapshots (Figure 4) from the LOP camera show the auroral activity in greater detail. In both cases, we used image differences to determine auroral features and dynamics more easily. Specifically, the upper keogram in Figure 3 shows the total brightness, while the bottom keogram shows difference images, with a 5 s lag. Similarly, the right parts in Figure 4 are differences of images shown on the left, also with a 5 s lag. Prior to auroral onset the equatorwardmost arc bifurcated and its equatorward portion moved to lower latitudes. Both arcs varied in intensity, but the major activation (accompanied by poleward expansion) at LOP started at 2107:08 UT. Enhanced auroras behind the active, poleward expanding aurora also expanded in the equatorward direction. Both keograms and individual TV camera and UVI (not shown) images show that the auroral bulge is a region of enhanced and strongly structured luminosity. The enhanced luminosity region of the bulge has a distinct equatorward

border, the EAB boundary that is not delineated by a discrete form, although some structures may occasionally appear here. The bright structures within the bulge proper appear like pulsating arcs and first started near the equatorward border of the enhanced precipitation at 2108:12 UT. After a few steps of poleward expansion (2110, 2113, 2117 UT) the auroral intensity in the bulge peaked while the equatorward propagation of the bulge slowed down (saturated) on a timescale of approximately 10 min. Following that, the luminosity started to decrease and the auroral features started to fade away. The structures inside the bulge proper have different geometries and propagation directions (mostly toward west, east, or equator) and variable appearances in the form of patches and arc segments (including north-south elements). While their investigation deserves further attention, it is beyond the scope of this paper. Here, we only emphasize the tendency for a predominantly equatorward motion of these structures, which are visible on the difference keograms as downward sloping auroral enhancements.

[10] In this event the availability of two meridionally separated TV cameras (at LOP and LOZ) allowed us to observe the breakup as well as the EAB near zenith for an extended period of time. The large-scale character of the equatorward expansion in this event is also supported by observations

## Loparskaya – 06.01.08

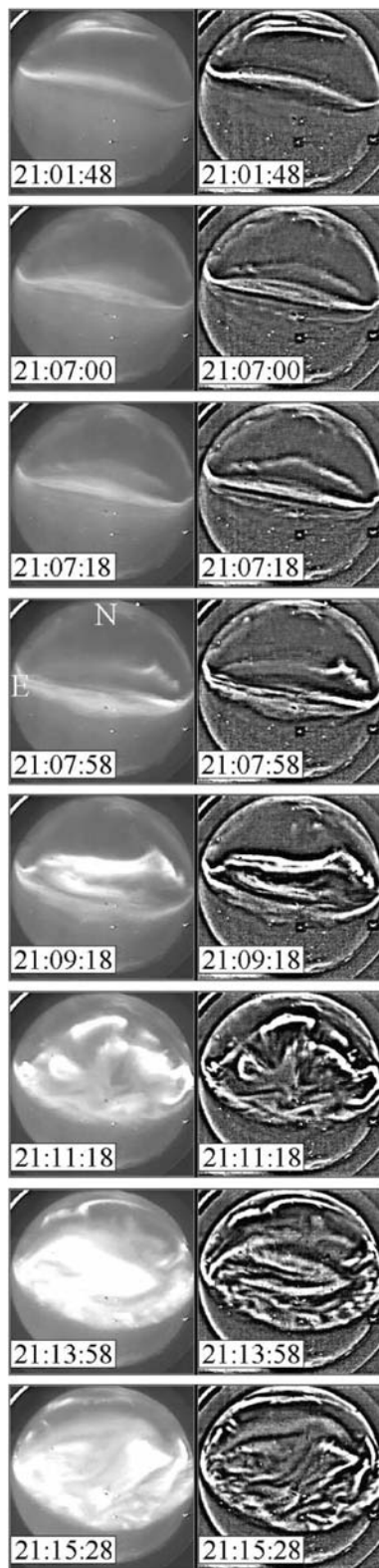


**Figure 4.** Examples of all-sky TV images, illustrating the development of auroras on 6 January 2008. Each part includes the (left) total brightness and (right) differential brightness images taken at the same time.

from two Finnish all-sky cameras, which documented the equatorward expansions down to about 100 km southward of Sodankyla (corrected geomagnetic latitude (CGLat) = 63.9°) and down to about 200 km southward from Kilpisjarvi (CGLat = 65.8°). Both Finnish cameras are located about 1 h MLT to the west of Loparskaya.

[11] During the second THEMIS conjunction, on 31 December 2007, there were two separate onsets: a small onset developing at around 1930 UT and a main substorm onset at 2007:40 UT (Figure 1). The second event was composed of a few well-defined individual activations, seen even in the AE index. The event was observed by the Polar UVI imager (data not shown), although the postmidnight half of the auroral oval was not covered by the instrument. Auroral activations were observed by UVI at 2007:49 (21–22 h MLT), 2012:30 (21–22 h MLT), 2025:20 UT (21–23 h MLT), and 2039:06 (00 MLT); the first two of them had clear effects in the inner magnetosphere.

[12] Figure 3 (bottom) displays the TV observations from Loparskaya. The observation conditions (breakup poleward of the station zenith) and the character of the auroral bulge development are similar to the previous event. First the pre-breakup arc structured (starting at about 2006:15), then a brightening was seen at its eastern edge (at about 2007:01), then the brightening propagated to the west and reached the LOP meridian at 2107:40 UT, and this signaled the major intensification, breakup, and poleward expansion.

[13] Multiple individual activations in the aftermath of onset, within the auroral bulge, are very distinct in this event. They can be distinguished as downward sloping auroral enhancements in the keograms. Two of the most distinct activations are seen to start at 2010 and 2012 UT and are denoted by blue traces a and b in the bottom part of Figure 3. These activations are seen starting at the poleward edge of the bulge and propagated toward the equatorward boundary, on occasion extending to even lower latitudes than the preexisting EAB and thus demarcating the new location of the EAB.

[14] Like in the previous event, the large-scale character of the EAB expansion is also supported by observations by the Finnish all-sky cameras, which documented the equatorward expansion of luminosity down to about 100 km southward of Muonio (CGLat = 64.7), situated about 1 h of MLT to the west of LOP (data not shown here).

[15] Two nearly simultaneous crossings of the developing auroral bulge were obtained by NOAA-POES spacecraft. The most interesting one was by NOAA 18 in the Southern Hemisphere. Its conjugate foot point in the northern ionosphere moved poleward through the field of view of the TV camera at LOP between 2016 and 2019 UT. Figure 5 (bottom) shows the precipitating integral energy flux in the range 0.3–20 keV, as well as precipitating and trapped energy flux of high energy particles. The unusually coincident flux enhancement of different species and energies on the equatorward side of the bulge crossing is collocated with the EAB, at 2016:25 UT. The boundary is observed at 65.1° CGLat (mapped to the northern hemisphere). Here, the precipitating electron energy flux in the 0.3–20 keV range shows an increase by an order of magnitude up to the 10 erg/cm<sup>2</sup> s level inside the auroral bulge. The energetic electrons above 30 and 100 keV are anisotropic but display enhanced and fluctuating precipitating fluxes (at 0°

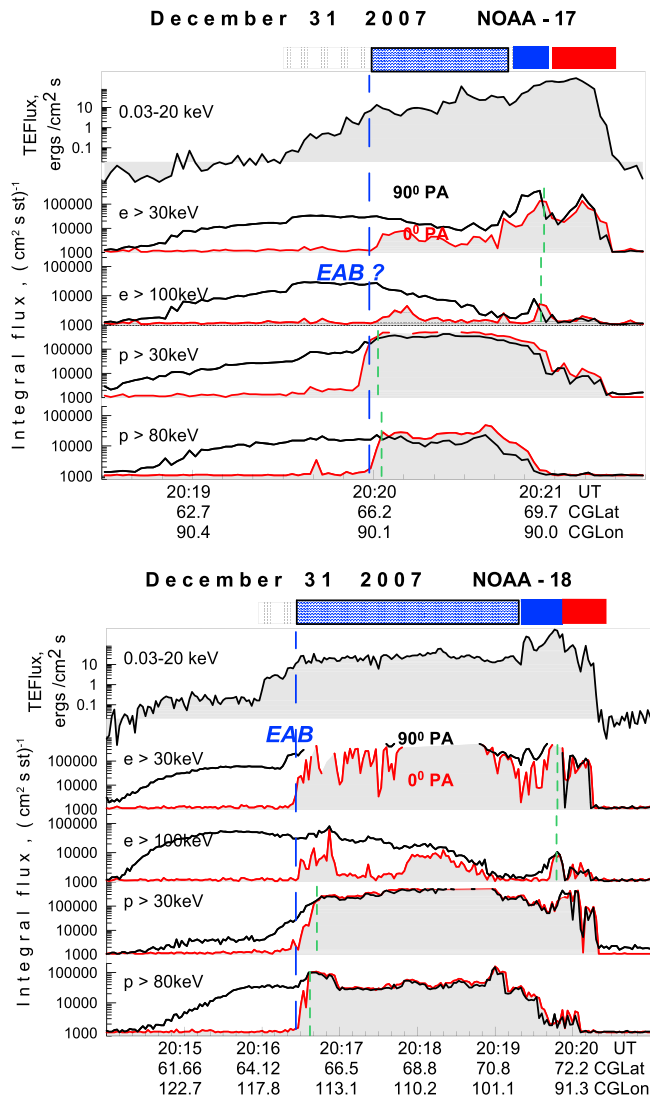


**Figure 5.** Observation of precipitated and trapped particle fluxes at NOAA 17 and NOAA 18 polar low-altitude spacecraft during the auroral expansion event on 31 December 2007. Corrected geomagnetic coordinates are given for the spacecraft foot point in the Northern Hemisphere; for comparison, the TV auroral observations are made at 115° CG meridian. The legend indicates different acceleration and precipitation domains according to *Sergeev and Kubyshkina* [1996]: red indicates the current sheet acceleration, blue indicates the acceleration in the newly dipolarized region, and hatched plateau precipitation indicates the main body of the dipolarized magnetic field region which is bounded from equatorward side by the EAB boundary.

PA) inside the bulge. The energetic protons show large isotropic fluxes within the bulge. The proton isotropy boundary (IB) is also located near the EAB. The auroral bulge is populated by enhanced but fluctuating electron fluxes up to very high energy. The characteristic energy of the total energy detector was about 18 keV for protons and about 8–11 keV for electrons (not shown).

[16] The other NOAA-POES spacecraft, NOAA 17, also crossed the auroral zone at around the same UT, but moved

in poleward direction in the Northern Hemisphere, 2 h MLT westward of the NOAA 18 crossing. It observed similar signatures, although the EAB at that MLT was about 1° CGLat poleward relative to the near-midnight value measured at NOAA 18 (Figure 5, top). Note that again, all channels exhibit a simultaneous flux increase near the equatorward boundary. It is also interesting to note that the proton IBs have an energy-latitude dependence that is opposite to what is commonly observed; that is, the 30 keV proton IB is located 0.2° equatorward of the >80 keV proton IB, whereas the typical behavior is that decreasing energies have IBs arranged in increasing latitudes, as was seen during the NOAA 18 crossing. This feature is extremely rare and indicates that the isotropic precipitation near this equatorward boundary was likely formed by wave-particle interactions which scatter particles into the loss cone rather than by a more general mechanism of nonadiabatic scattering in the tail current sheet [e.g., *Sergeev and Kubyshkina*, 1996]. It indicates that very effective particle scattering mechanisms likely operate near the EAB boundary in the equatorial magnetosphere. As seen in NOAA 17, the proton precipitation into the bulge seen on NOAA 18 also displays a plateau in flux while both ion and electrons are rather energetic; the peak energy flux was at 11–16 keV for protons and at 2–3 keV for electrons (not shown).

### 2.3. Magnetospheric Observations Near the Substorm Onset

[17] Figure 6 shows THEMIS observations of the magnetic field, plasma, and energetic particle flux during the first substorm. The outermost probe P2 was at  $r \sim 10.5 R_E$  in the southern plasma sheet boundary near onset. As a consequence it did not observe strong plasma flows. The earliest feature to notice was a drop of the total (magnetic+plasma) pressure and an increase of the  $B_x$  and  $B_z$  components of the magnetic field, which all started at about 2104:40 UT. We interpret this as a signature of plasma sheet expansion and the start of the unloading phase in the tail, consistent with recent statistical results by *Miyashita et al.* [2009]. The earliest breakup determination at 2107:08 (TV at LOP) and 2107:01 (Polar UVI) is delayed by about 2 min after this time.

[18] The innermost THEMIS probe P5 crossed the inner boundary of the electron plasma sheet at about  $4.8 R_E$ , 22.4 h MLT at around 1930 UT (as observed by the ESA instrument), moving outbound through the middle of the inner plasma sheet. It was at  $6.9 R_E$  distance at the time of substorm onset. P5's observations are a bit complicated since the injection features in energetic protons and electrons as well as the dipolarization signatures were all observed at different times. The first one was a smooth flux increase in the lowest energy (about 28 keV) proton SST channel, observed at 2106:10. At this time about 1 min period oscillations of plasma flows also started (with only about 10 km/s amplitude, not shown). A clear flux increase was seen in the low energy SST electron channels combined with a drop at the electron energies above 200 keV at 2108:10 UT; it was not accompanied by corresponding proton flux increase. These are typical signatures of dispersionless electron injections, observed at the dawnside flank of the injection region [*Birn et al.*, 1997]. At this time the dipolarization was not yet observed, as the  $B_z$  component rather decreases (note

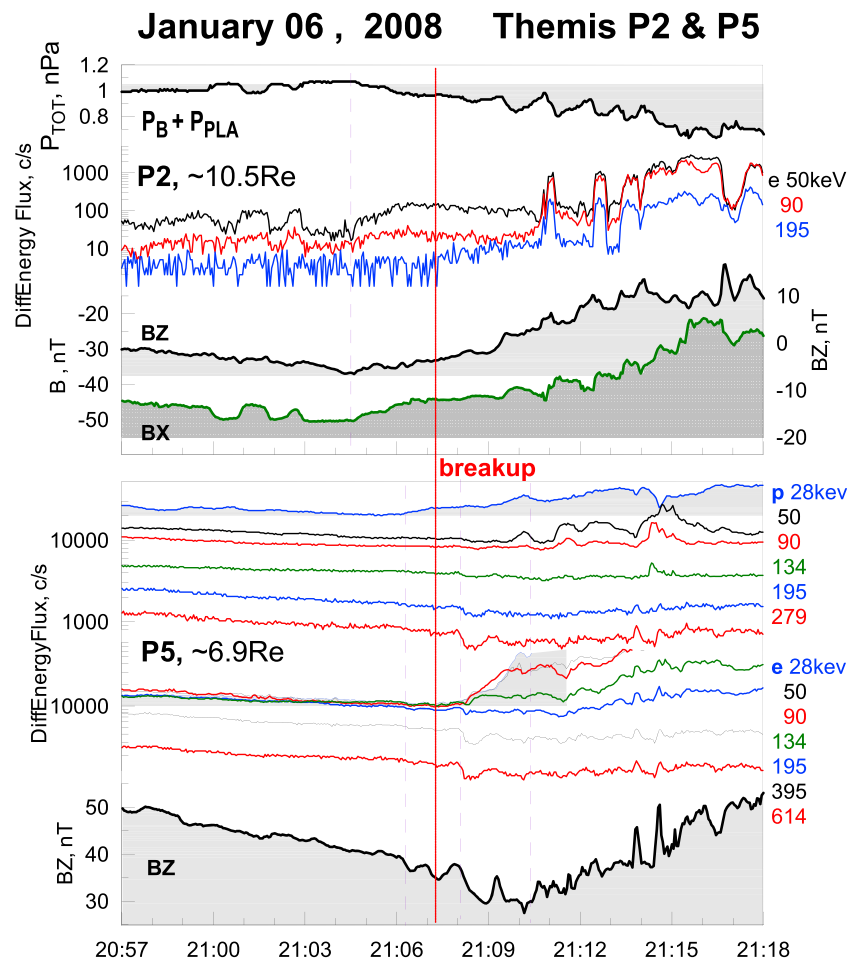


**Figure 6.** THEMIS observations (top) near the plasma sheet-lobe boundary at about  $11 R_E$  distance (P2 spacecraft) and (bottom) in the near-geosynchronous region (P5 spacecraft) during the 6 January 2008 substorm. Red line indicates the time of auroral breakup, and other dashed vertical lines indicate other times of interest (see Table 1 for timing information).

that  $B_z > |B_x|$ ), exhibiting superimposed about 1 min period oscillations.  $B_z$  gradually starts to increase after 2110:20 UT, the increase lasting for 10 min. The strong  $B$  field fluctuations superimposed on top of this  $B_z$  increase are associated with modulations of the energetic particle flux; they may contribute to the structure of auroral precipitation.

[19] The general magnetospheric features and relative timing during the 31 December 2007 substorm are similar to the 6 January 2008 one (Figure 7). The outermost THEMIS probe P1 was at the lobe-plasma sheet boundary, at  $r \sim 11.8 R_E$  distance, near the main onset. P1 observed the start of unloading (decrease of the total pressure) at 2006 UT, while the  $B_z$  increase started a minute later. There was one more activation at about 2012 UT shown by the second dashed vertical line, and this activation sequence nicely corresponds to the second electron injection at about 20:14 UT on P2, located in the inner magnetosphere.

[20] The inner THEMIS probe P2 crossed the inner boundary of the electron plasma sheet at about  $5.8 R_E$ , 22.7 h MLT at around 1930 UT. By the time of substorm onset, it was near  $6.9 R_E$  at the 23.1 h MLT meridian. Like in the previous case, the earliest tail signature is a 28 keV proton flux increase which starts gradually, not later than

2007:30 UT (but 1.5 min after the unloading signature commenced at P1). The two-step  $B_z$ -component increase (against its decreasing trend on the outbound trajectory) started at 2009:00 UT and became more abrupt at 2013:40 UT. Corresponding high energy electron injections started at 2010:20 (dispersionless) and again at 2014 UT (evidently with a weak energy dispersion). Both electron injections were not accompanied by proton injection, which is common for observations at the dawnside of the injection center. Closer to the Earth, at  $6.6 R_E$ , the effects of two electron injections were observed by the LANL-02A spacecraft positioned at 00.5 h MLT, about 1.5 h MLT dawnward of P2 (Figure 7, bottom). Here, both injections displayed an energy dispersion (which was larger for the second injection). From the dispersion, we inferred the injection times to have occurred at about 2011 and 2014 UT at earlier local times, i. e., consistent with the timing and location of the injections observed at P2.

#### 2.4. Magnetic Mapping

[21] The  $B_x$  and  $B_z$  magnetic field components observed by the two THEMIS probes, together with the values of the field predicted by the models, are plotted for the 6 January

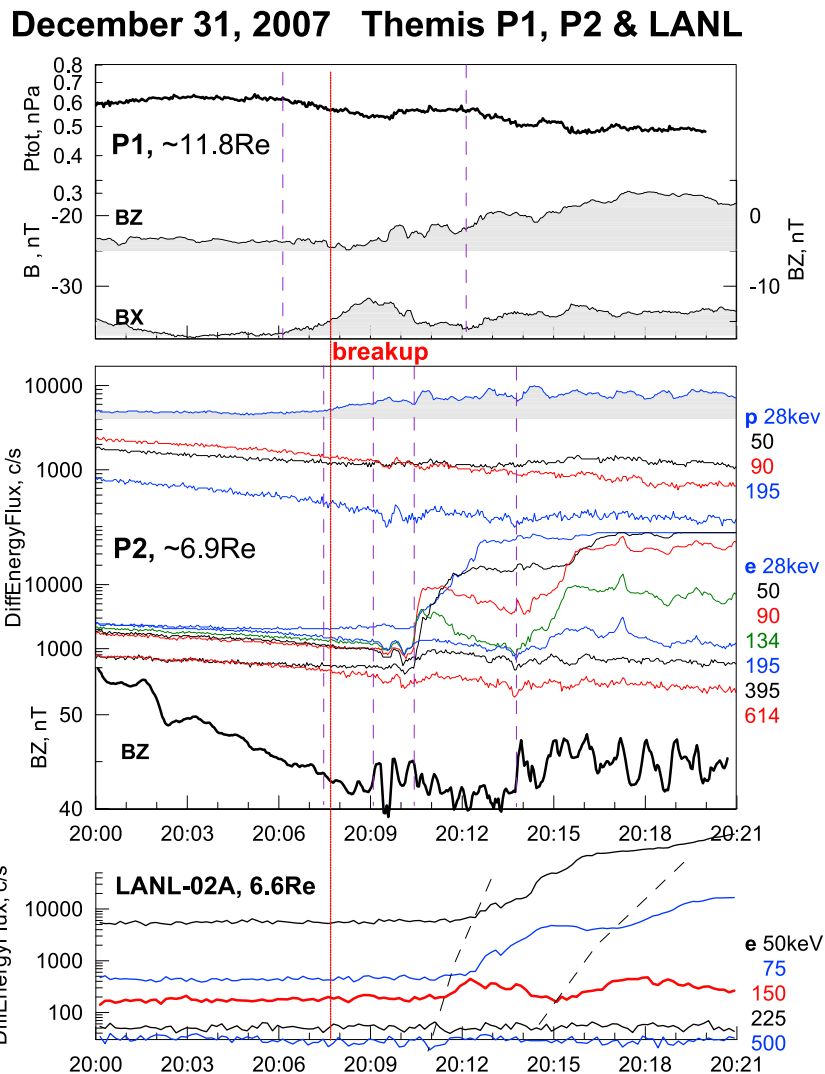


**Figure 7.** THEMIS observations (top) near the plasma sheet–lobe boundary at about  $12 R_E$  distance (P1 spacecraft) and (bottom) in the near-geosynchronous region (P2 and LANL-02A spacecraft) and during the 31 December 2007 substorm.

2008 substorm in the bottom part of Figure 8. Only the external part of the magnetic field is shown (i.e., the International Geomagnetic Reference Field (IGRF) contribution was subtracted from both data and models) in order to better resolve the variations, which would otherwise be dominated by the spacecraft motion in the strong dipole field. The standard T96sw model is computed based on 5-min-averaged, propagated solar wind interplanetary magnetic field (IMF) parameters ( $P_d$ ,  $B_y$ ,  $B_z$ ) available from the OMNI data set. This model predicts the approximate value of the observed field but fails to reproduce the considerable magnetic variations observed before and after the substorm onset. Another model, AM-01 [Kubyshkina *et al.*, 2009] is obtained by varying the T96 input parameters to achieve the best fit to the magnetic fields observed by the five THEMIS probes (avoiding the  $r < 5 R_E$  near-perigee region). Both models are routinely computed at 5 min time resolution for the THEMIS tail season and are available at [http://geo.phys.spbu.ru/themis/models\\_public](http://geo.phys.spbu.ru/themis/models_public). The AM-01 model reproduces the observed variations much better than the T96 model, particularly the  $B_z$  decrease

(P5, P2) and  $|B_x|$  (P2) increase, corresponding to magnetic field stretching prior to the onset. Moreover, as the  $B_z$  (P5, P2) increase and  $|B_x|$  (P2) decrease after substorm onset, corresponding to the typical field dipolarization at substorm expansion phase, AM-01 again models these signatures with high fidelity compared to the standard T96 model. AM-01 therefore makes it possible to estimate the variations of spacecraft foot point locations at around the substorm onset relative to the predictions of standard model. The CG latitudes of the ionospheric foot point of the P5 spacecraft are shown in the top part of Figure 8 using both models. Compared with the smooth trace predicted by the T96 model, the  $B$ -field-adapted AM-01 model predicts an ionospheric foot point for  $2^\circ$ – $3^\circ$  lower latitude prior to substorm onset (due to the stretched configuration) and  $2^\circ$ – $3^\circ$  higher latitude after substorm onset (due to dipolarization). The entire latitudinal variation of the spacecraft foot point due to the changing magnetic configuration can be as large as  $5^\circ$ – $6^\circ$  around the substorm onset. This clearly demonstrates the importance of constructing adaptive models

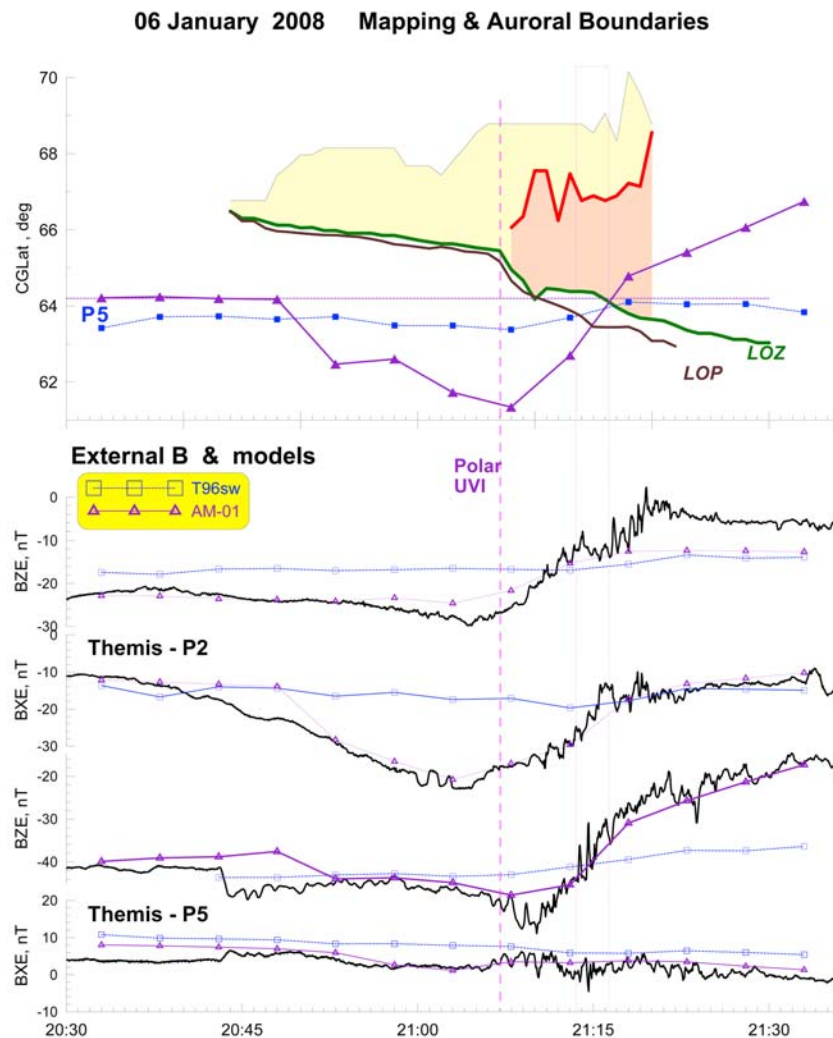


**Figure 8.** (top) Corrected geomagnetic latitudes of the equatorward auroral boundaries observed at LOP and LOZ, together with time variations of ionospheric foot point of the innermost THEMIS spacecraft. The latitudes of polewardmost arc and of the breakup arc (red) are also shown. (bottom) Magnetic field  $B_x$  and  $B_z$  components (dipole contribution subtracted) observed by two near-midnight THEMIS probes as well as the same components as predicted by solar wind-based T96 model and by the AM-01 model adapted to fit THEMIS observations.

when doing mapping both prior to the substorm onset and after the onset.

[22] The CG latitudes of the bulge's equatorward boundary (EAB) and of other auroral boundaries, including the breakup arcs and the poleward arcs, are also shown on this plot for comparison. They are obtained from the location of the lower border of the auroral forms in the keograms of LOP and LOZ stations, under the assumption that the lower altitude of auroras is 110 km, followed by a conversion of geographic to CG coordinates. Although the meridians of the two stations are very close in longitude ( $3^\circ$  longitude difference), and the stations are separated by only about 80 km along the meridional direction, the EAB determinations may differ at times by as much as  $0.7^\circ$  CGLat. We attribute this to the complex shape of the boundary and/or the variations in the actual altitude of the auroral emissions in the auroral bulge. For example, on the basis of the hard spectra of the precipitating electrons measured at NOAA 18 it is possible

that on occasion the auroral luminosity lower border is below 100 km in altitude. With two models and two determinations of the EAB location, the time interval when the P5 foot point crosses the EAB location is predicted to be between 2113 and 2117 UT (Figure 8, top). During this time the  $B_z$  component at P5 was increasing, starting gradually at about 2111 UT. Impulsive  $B_z$  increases start at 2115 UT. There is no single feature which we can definitely associate with a sharp EAB boundary, a point that we shall examine again in section 3.

[23] Similar analysis for the 31 December 2007 substorm results in Figure 9. In this case the standard AM-01 fails to reproduce the dipolarization as clearly, probably because of the smaller magnitude of variations compared with the 6 January 2008 substorm. We repeated the adaptive procedure by increasing the weight of the P2 magnetic field input by a factor of 3 compared with other spacecraft. The resultant model (AM-01c) more closely follows the  $B_z$  variation

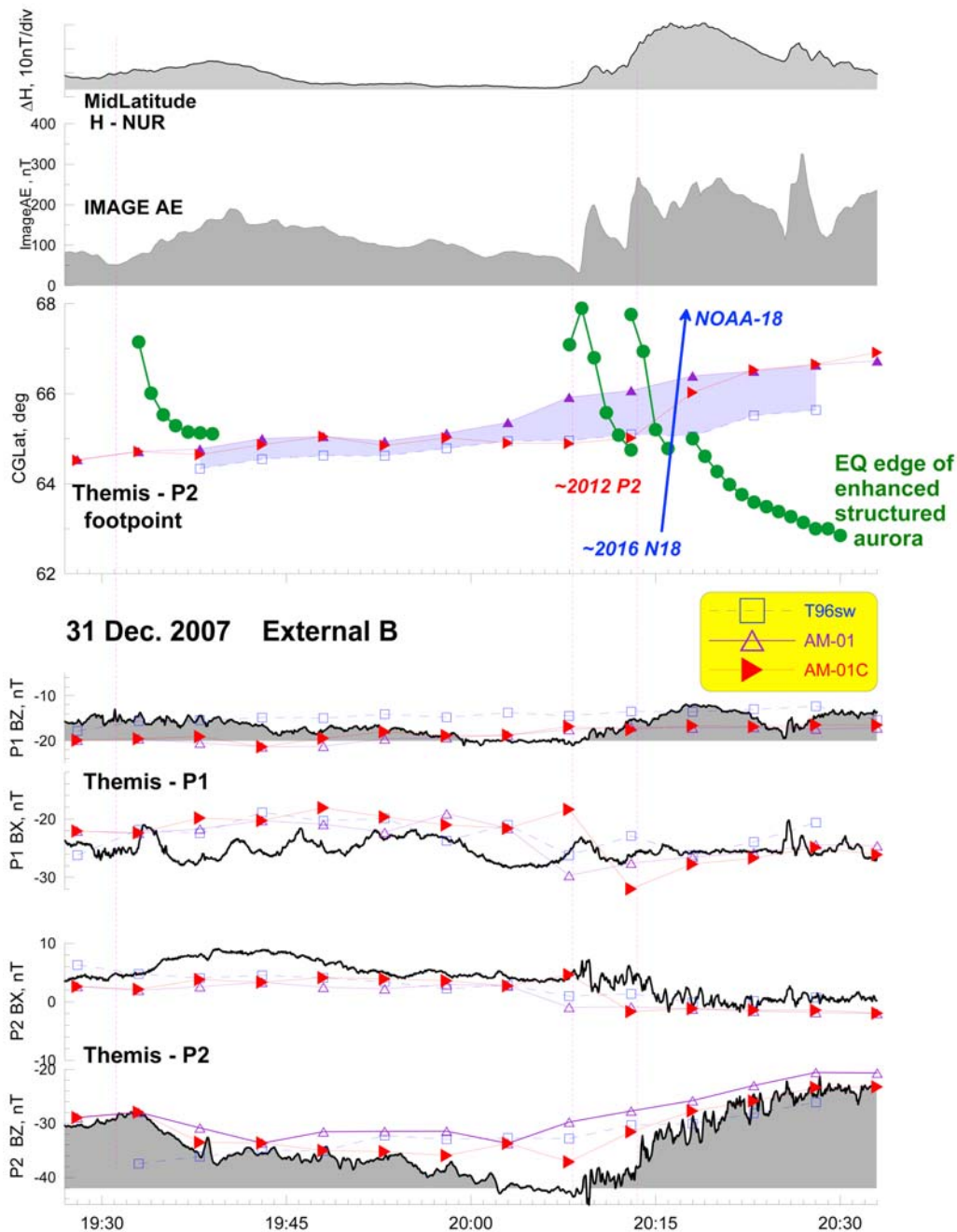


**Figure 9.** Same as in Figure 8 but for the 31 December 2007 substorm. Image AE and magnetic H-component variation in Nurmijarvi are also shown for reference to emphasize the impulsive development.

at P2, although the agreement with the observed magnetic field is still not as good as in the previous event. We notice, however, a reasonably good agreement between predicted and observed external contributions for all models (within about 5 nT difference for 20–40 nT inputs), which means that the models still provide a reasonable basis for mapping. The auroral response in this case displays a few traces of downward sloping auroral enhancements seen on both the total and differential brightness keograms as mentioned earlier (Figure 3, bottom). The two clearest traces a and b correspond to two intensifications of the westward electrojet as evidenced in the Image AE index (Figure 1). The intensifi-

cations correspond to the times of the double dipolarization and double electron injection observed at P2 and LANL-02A (Figure 7). According to Figure 9, these auroral features cross the predicted locations of P2 foot points at 2011–2012 and at 2014–2015 UT, which is in a good agreement with onsets of two dispersionless injections at 2011 and 2014 UT at that spacecraft, and the associated  $B_z$  increases.

[24] We note in passing that earlier in this event, another breakup with a clear trace of equatorward moving auroral brightness increase was recorded at 1930 UT (evident in Figure 4). According to our models, this trace approaches but does not cross the modeled P2 foot points. No signs

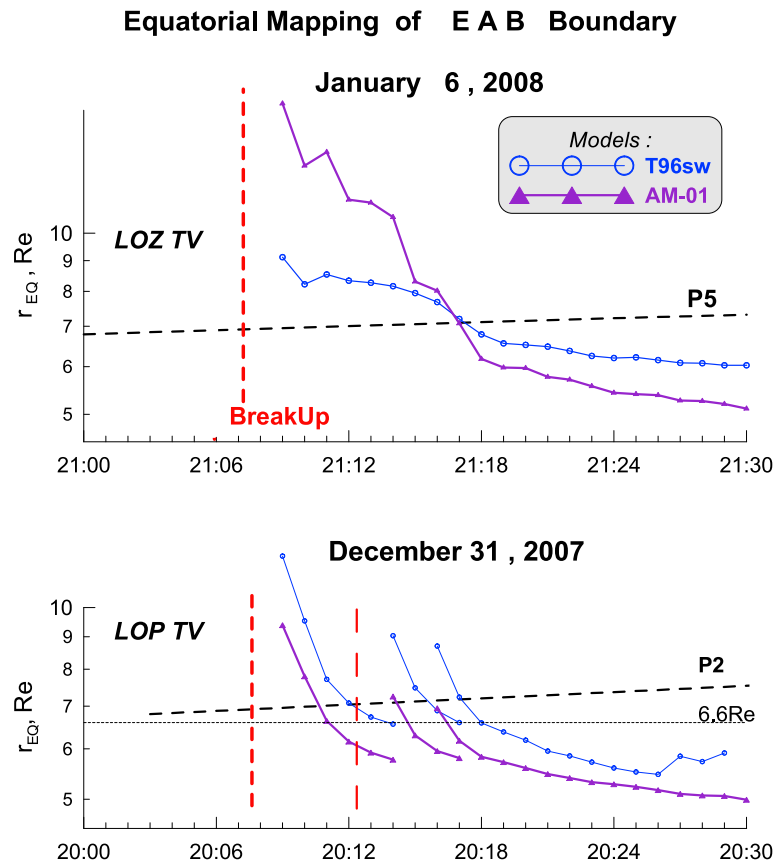


**Figure 10.** Mapping of the equatorward boundary of the active auroras to the equatorial near-midnight magnetosphere using both standard and adapted models.

of dipolarization at P2 and no comparable injection at LANL spacecraft were observed. This provides further support for our interpretation of the equatorward moving auroral structures as the ionospheric manifestation of the earthward moving injections and dipolarizations.

[25] The mapping of the EAB to the magnetosphere for both events is shown in Figure 10. The difference between the standard and adapted models is significant: The innermost penetration distance varies by  $1 R_E$  at  $r \sim 5\text{--}6 R_E$  and the velocities of the inward motion of the boundary differ by a factor of 2 at about  $7 R_E$  distance where the innermost THEMIS probes are located. Using the adaptive model we estimate these velocities to be about 100 km/s, which is consistent with previously reported velocities of dipolarization fronts at  $7\text{--}9 R_E$  [Ohtani, 1998; Apatenkov *et al.*, 2007].

### 3. Discussion

#### 3.1. EAB and Its Magnetospheric Counterpart

[26] The two events analyzed indicate that following a substorm onset an area of active auroras is formed in the wake behind the poleward expanding discrete auroral forms, forming the auroral bulge proper, which is expected to be the ionospheric counterpart of the plasma sheet that is energized during the substorm [Yahnin *et al.*, 2006]. These auroras typically appear in the form of enhanced precipitation which contains complex and dynamic embedded structures.

[27] Particularly, the bulge includes distorted arcs, patches, and arc fragments (Figure 4), including elements of north-south arcs [see also Nakamura *et al.*, 1993]. Under favorable observing conditions, with active auroras starting (breakup) in the northern sky, these enhanced auroras display a distinct EAB boundary, which progressively expands in the equatorward direction. Distinct from the poleward boundary of the bulge, this EAB boundary is not delineated by any single arc-like structure (though equatorward moving arcs may reach it and redefine its location), but rather looks like a boundary between undisturbed and activated precipitation regions (see, e.g., the individual images in Figure 4). Initially the speed of equatorward expansion is rather large (30–50 km/min, Figures 8 and 9) and then it slows down. The development can be nonmonotonic in the case of several distinct injections. The timescale of the major development of the EAB is about several to 10 min; on this timescale, the equatorward motion of the EAB stops and the intensity of precipitation fades away.

[28] The equatorward expansion of the EAB has been previously reported by many observers who presented their auroral data in a keogram format, although it did not attract as much interest as the poleward boundary. The interpretation of the EAB was not conclusive because of mapping uncertainties and the general lack of concurrent near-Earth spacecraft observations. Eather *et al.* [1976] analyzed auroral observations made near the foot point of geostationary ATS-5 spacecraft. During moderate and strong activity they

observed energetic flux enhancements at ATS-5 (plasma injections) in association with auroral enhancements propagating equatorward. They suggested that their equatorward border is the precipitation from the injection boundary [McIlwain, 1974], a phenomenological construct whose detailed physics was unknown at that time, but which can now be associated with the intrusion from the magnetotail of the fast flows generated by reconnection or other mechanism (see, e.g., the simulations by Birn *et al.* [1998]). Close association between multiple auroral activations and multiple electron injection to geostationary orbit was mentioned by Nakamura *et al.* [1991]. Using TV observations of small substorms Nakamura *et al.* [1993] also confirmed that the auroral features within the poleward expanding bulge systematically develop toward west, east, and equatorward from the breakup region and emphasized that the north-south auroras participate in the equatorward expansion. This is close to what we observed, although in our observations the north-south forms appear as an occasional detail, which may or may not be present at any specific time during the equatorward progression of the EAB.

[29] Our study suggests that the EAB is not identical to the inner plasma sheet (PS) boundary, as suggested in some early studies. This is most clearly evidenced in the first substorm event, in which the electron boundary was crossed at  $4.9 R_E$ , prior to the substorm, whereas the EAB developed in the middle of the inner plasma sheet for the first 10 min after the breakup, and it could only reach the inner boundary location not earlier than about 20 min after the onset (Figure 10). The EAB can, however, propagate down to (and pass inward of) the previous inner plasma sheet boundary as evidenced during our second substorm, so it can contribute to the rapid and large-scale inward motion of the inner PS boundary observed during the substorm expansion [Runov *et al.*, 2008]. This interaction is an interesting topic for future studies.

[30] The EAB, as viewed in the ionosphere, is akin to a precipitation boundary (but not necessarily the acceleration boundary). Its distinct particle property is the rather high energy of the precipitating electrons, being about approximately 10 keV in the case of NOAA 18 and 2–3 keV in the case of NOAA 17 observations presented in Figure 5. The bulge proper also includes considerable energetic particle precipitation; in our cases the  $>30$  and  $>100$  keV ions were isotropic whereas the energetic electrons were anisotropic and their fluxes are more structured and increased almost (but not quite) up to levels of the trapped fluxes.

[31] The equatorward expansion has a relatively large size in MLT and can be seen in global auroral images (see Figure 2, top) even if such images may not have sufficient spatial resolution (about 100 km) to explore the details. Nearly simultaneous detection of the equatorward auroral expansion by a few all-sky cameras distributed over more than 1 h MLT sector, mentioned in section 2.2, confirms a nonlocal appearance of the EAB on the auroral bulge scale, although the details of dynamics on a global scale still have to be explored, especially in the case of multiple injections.

[32] Individual auroral activations contribute, on occasion, to the EAB location and motion, as was most clearly observed during the 31 December 2007 event. Each next activation, following the initial breakup, starts to develop at the poleward boundary of the bulge and then propagates equator-

ward for several minutes passing through almost the entire bulge before reaching the area where the previous activation saturated. The multiplicity of the downward sloping auroral enhancements on the keograms during strong injections was noticed by Eather *et al.* [1976]. This description is similar to the dynamics of the poleward boundary intensifications (PBI) [Lyons *et al.*, 2000; Zesta *et al.*, 2006] or the auroral streamers [Sergeev *et al.*, 2000], except that the above mentioned studies emphasized their origin at the poleward oval boundary (the polar cap boundary) and subsequent equatorward motion, but did not consider the final stage of the streamers. In our case, the arc activations within the bulge pertain to the initial expansion phase of the substorm and are contained within the active substorm region; that is, they are not late substorm expansion or recovery-type phenomena as the PBIs. The later stage of PBI/streamer intrusion has been investigated in one case by Kauristie *et al.* [2003], who documented enhanced luminosity with embedded dynamical structure as well as evidences of azimuthal deflection of the injected accelerated plasma near the low-latitude termination of the streamer intrusion. However, one important difference to the bulge streamers is that, unlike the EAB, the PBIs/streamers have a limited longitudinal extent, being about 300–400 km scale across the structure in the Kauristie *et al.* [2003] case. The EAB can be understood as the integral effect of multiple injections, some of which are intense and discrete enough to be clearly observed.

[33] Our results confirm a close relationship between individual auroral injections contributing to the EAB formation and dipolarizations and plasma injections observed in the conjugate inner magnetosphere, as was previously noticed also by Nakamura *et al.* [1991]. This is most evident in the second substorm event which exhibited a double injection at THEMIS P2 and at LANL-02A spacecraft. The onset of magnetic and particle injection signatures in the magnetosphere coincides to within 1 min with the time of EAB passing over the P2 foot point (Figure 7). This association is what we expect based on a simple acceleration model, taking into account that the magnetic field increase in the magnetosphere (spatial or temporal) is related to the betatron and Fermi particle acceleration and that precipitation of energized plasma behind the magnetic field discontinuity will contribute to the enhanced and structured auroral luminosity. Both  $B_z$  and electron fluxes show considerable short-scale variations which may be the manifestations of spatial structuring of auroral precipitation seen in Figures 3, 4, and 5.

[34] The situation is more complex, however, during the 6 January 2008 substorm event because there the dipolarization front was not as sharp and is delayed relative to the injection of energetic electrons by about 2 min (Figure 6). A possible explanation for this apparent inconsistency to our model is that the observation point was at the dawn flank of the injection, as suggested by the absence of comparable ion flux increase during dispersionless electron flux increase and by the auroral imager data in Figure 2. This is supported by a reconstruction of the SCW from midlatitude magnetic variation, which provides the location of SCW downward current at 23.5 h MLT. Thus initially P5 was likely just outside of the injection-SCW region, observing only a weak negative  $B_z$  perturbation and drifting electrons accelerated from a nearby but nonlocal source.

**Table 1.** Substorm Onset and Injection Timing

Feature	6 January	31 December
Breakup	2107:08	2007:01
InnerMSP	P5	P2
P-growth	2106	2006
e-Injection	2108	2010:20/2014:00
+ $\delta$ BZ	2110–2011	2009:00/2013:40
Distance	6.9 $R_E$	6.9 $R_E$
Predicted EABcross	2113–17	2010–11/2014–15
OuterMSP	P2	P1
+ $\delta$ BZ	2105?	2007?/2012.5
Ptotdrop	b21:04:40	2006/2012.5
Distance	10.5 $R_E$	11.8 $R_E$

[35] Supporting this interpretation is also the realization that while in auroral records the EAB is a well-defined 2-D boundary, a few tens of kilometers across, an associated sharp structure was not observed on P5. The  $B_z$  increase (dipolarization) is not sharp, it continues for about 8–10 min, and a spatial interpretation of the  $B_z$  variation would result in a radial scale being of the order of about 5  $R_E$ , i.e., inconsistent with the mapped scale size of the EAB. A non-local dipolarization front explains this inconsistency: if the dipolarization front (sharp spatial boundary) was not crossed at this location, then the  $B_z$  increase can be interpreted as a temporal variation due to the global relaxation of the magnetotail. Moreover, the sharp electron injection at P5 comes too early to be interpreted as a propagating EAB at P5's location because the P5 foot point at 2108 UT was 2°–3° CGLat below the EAB location (Figure 8). One may speculate that both difficulties can be due to the proximity of the SCW downward current, which is absent in the adaptive model, but which can considerably distort the mapping. We conclude that this is a tentative explanation and that more events with observations in the middle part of the SCW have to be analyzed to finally identify the magnetospheric counterpart of the EAB.

### 3.2. Timing of Substorm Onset and Injections

[36] The TV cameras were well positioned to observe the auroral onsets during the two isolated substorms studied, and there were two THEMIS probes at the same meridian in the near-geosynchronous region as well as near the plasma sheet boundary at  $r \sim 11 R_E$  (Figure 1). The timing results summarized in Table 1 are similar in both events. In every case the auroral onsets were preceded by a total pressure drop (unloading onset) at about 11  $R_E$ . Note that the associated decrease of  $|B_x|$  and increase of  $B_z$  were the first manifestations to be observed in both cases. The major brightening of the auroral arc (auroral breakup) followed 1–2 min after the start of lobe energy unloading. The earliest injection or dipolarization signatures at  $r \sim 7 R_E$  were observed 1–2 min after the breakup, which is consistent with an average 1.8 min time lag of geosynchronous particle injections after the auroral breakup observed by Polar UVI reported by *Liou et al.* [2001]. Our study suggests that this time lag characterizes the inward propagation of the injected particle cloud. The earliest signature at about 7  $R_E$  was, however, observed much earlier; it was a smooth growth

of about 30 keV proton flux, presumably signaling the growth of plasma pressure. Consistent with results by *Nishimura et al.* [2008] and *Sergeev et al.* [2008], this may indicate the early arrival of the fast wave launched by the inward injection of an accelerated plasma cloud. An extended discussion of the timing interpretation is beyond the scope of this paper, yet we present this material herein for the benefit of future statistical studies.

### 3.3. Significance of Accurate Mapping

[37] The magnetospheric configuration undergoes large changes before and after the substorm onset, which makes the interpretation of auroral dynamics in terms of magnetospheric processes difficult. In the inner magnetosphere the magnetic field is stretched before the expansion onset, and it is dipolarized after the onset, so the mapping may not be accurate with existing standard empirical models. The mapping error was, however, unknown, but it was a general opinion that it is not as large (about 1° of latitude) if mapped to the ionosphere from the geosynchronous distance. In our study we are able to construct a time-dependent THEMIS data-based model [*Kubyskhina et al.*, 2009]. During the first intense substorm (AE  $\sim$  600 nT), we are able to reproduce the values and variations of the magnetic fields measured at P2 and P5 fairly well (Figure 8) and obtain the following results. First, the P5 foot point variations (starting from  $r \sim 7 R_E$ ) are large, about  $\mp 3^\circ$  CGLat, within  $\pm 30$  min from  $T_0$ , i.e., during the growth and expansion phases. Accordingly, the total variation of the spacecraft foot point latitude is as large as 5°–6° CGLat, which is about the size of the field of view of one all-sky camera in the ionosphere. Second, the spacecraft foot point moves nearly at the same speed as the EAB boundary moves (see Figure 8), so the actual velocity of the inward injection in the magnetosphere is roughly twice as large compared to the EAB mapping velocity in stationary magnetospheric models (Figure 10). The importance of constructing time-dependent models when studying the substorm phenomena, by using coordinated ground and spacecraft observations, like in the THEMIS system, is well illustrated by this example.

[38] Such extreme mapping distortions may explain the seeming contradiction between recent THEMIS observations of midtail onset location [e.g., *Angelopoulos et al.*, 2008] and a near-Earth inference of onset mapping derived solely from ground currents or images [e.g., *Rae et al.*, 2009].

## 4. Conclusion

[39] Using conjugate observations in the ionosphere and magnetosphere, we show that the enhanced structured auroras activated after the breakup have a well-defined EAB boundary which expands equatorward with an initial speed exceeding 30–50 km/min and then gradually stops (saturates). Multiple activations can participate in the EAB formation. Low-altitude satellite observations confirm that precipitated electrons are accelerated over the auroral bulge and have a clear equatorward termination. The mapping of the EAB to the magnetosphere indicates its inward motion at a velocity decreasing with the decreasing distance from the Earth and about 100 km/s at  $r \sim 7 R_E$ , which is consistent with previous velocity estimates of the earthward moving sharp

dipolarization or injection front. In one event (31 December 2007) this dipolarization and injection front was observed at the location and time predicted by the mapping of EAB structure into the ionosphere. In another event we report a nontypical observation of the dipolarization and injection signatures which do not coincide with each other and have no classic dipolarization front; this was tentatively explained by the location of the inner magnetospheric spacecraft outside the SCW (on the dawnside, consistent with the observation of drifting electron injection). By using the model adapted to THEMIS magnetic observations we illustrate the importance of time-dependent variations of the magnetic field and of the ionosphere-magnetosphere mapping, with variations of mapped latitude being as large as  $5^{\circ}$ – $6^{\circ}$  CGLat from the geosynchronous distance during the relatively modest substorm event. We conclude that studies of auroral processes complemented by adapted time-dependent magnetospheric modeling can be a valuable tool for investigating the inward penetration of plasma injections as well as the onset and dynamics of the auroral structures. Such a study should cast light on the nature of particle energization and heating inside the dipolarization region as well as the location and physical process governing substorm initiation.

[40] **Acknowledgments.** Data from the MIRACLE geophysical network in Scandinavia are made available by Finnish Meteorological Institute. NOAA-POES SEM-2 data (D. Evans, PI) are made available by NOAA and energetic particle data of LANL spacecraft (R. Belian, G. Reeves, PI) are provided by the LANL Web site. The OMNI data base is run by the NGDC at NASA Goddard Space Flight Center. We thank all data providers for their valuable data sets. Thanks to K. H. Glassmeier, U. Auster, and W. Baumjohann for the use of FGM data provided under the lead of the Technical University of Braunschweig and with financial support through the German Ministry for Economy and Technology and the German Center for Aviation and Space (DLR) under contract 50 OC 0302. We thank A. Nikolaev and S. Apatenkov for their help in data processing, M. Kholeva for help in preparing the manuscript, and T. Kozelova for the discussions. The work was supported by THEMIS contract NAS5-02099. The work by V.S. and M.K. was also supported by Russian Ministry of Science grants and by RFBR grants 07-02-91703 and 10-05-00223.

[41] Amitava Bhattacharjee thanks Donald Fairfield for his assistance in evaluating this paper.

## References

- Akasofu, S.-I. (1964), The development of auroral substorm, *Planet. Space Sci.*, *12*, 273–282.
- Akasofu, S.-I. (1977), *Physics of Magnetospheric Substorms*, p.274, D. Reidel, Norwell, Mass.
- Angelopoulos, V. (2008), The THEMIS mission, *Space Sci. Rev.*, *598*, 5–34, doi:10.1007/s11214-008-9336-1.
- Angelopoulos, V., et al. (2008), Tail reconnection triggering substorm onset, *Science*, *321*, 931–935, doi:10.1126/science.1160495.
- Apatenkov, S. V., et al. (2007), Multi-spacecraft observation of plasma dipolarization/injection in the inner magnetosphere, *Ann. Geophys.*, *25*, 801–814.
- Birn, J., M. F. Thomsen, J. E. Borovsky, G. D. Reeves, D. J. McComas, and R. D. Belian (1997), Characteristic plasma properties of dispersionless substorm injections at geosynchronous orbit, *J. Geophys. Res.*, *102*, 2309–2318.
- Birn, J., M. F. Thomsen, J. E. Borovsky, G. D. Reeves, D. J. McComas, R. D. Belian, and M. Hesse (1998), Substorm electron injections: Geosynchronous observations and test particle simulations, *J. Geophys. Res.*, *103*, 9235–9248.
- Eather, R. H., S. B. Mende, and R. J. R. Judge (1976), Plasma injection at synchronous orbit and spatial and temporal auroral morphology, *J. Geophys. Res.*, *81*(16), 2805–2824.
- Evans, D. S., and M. S. Greer (2006), Polar Orbiting Environmental Satellite Space Environment Monitor: 2. Instrument Descriptions and Archive Data Documentation, technical memorandum, Natl. Oceanic and Atmos. Admin., Silver Spring, Md.
- Kauristie, K., V. A. Sergeev, O. Amm, M. V. Kubyshkina, J. Jussila, E. Donovan, and K. Liou (2003), Bursty bulk flow intrusion to the inner plasma sheet as inferred from auroral observations, *J. Geophys. Res.*, *108* (A1), 1040, doi:10.1029/2002JA009371.
- Kornilova, T. A., I. A. Kornilov, and O. I. Kornilov (2008), Fine structure of breakup development inferred from satellite and ground-based observations, *Ann. Geophys.*, *26*, 1141–1148.
- Kubyshkina, M., V. Sergeev, N. Tsyganenko, V. Angelopoulos, A. Runov, H. Singer, K. H. Glassmeier, H. U. Auster, and W. Baumjohann (2009), Toward adapted time-dependent magnetospheric models: A simple approach based on tuning the standard model, *J. Geophys. Res.*, *114*, A00C21, doi:10.1029/2008JA013547.
- Liou, K., C.-I. Meng, P. T. Newell, A. T. Y. Lui, G. D. Reeves, and R. D. Belian (2001), Particle injections with auroral expansions, *J. Geophys. Res.*, *106*, 5873–5881.
- Lyons, L. R., E. Zesta, J. C. Samson, and G. D. Reeves (2000), Auroral disturbances during the January 10, 1997 magnetic storm, *Geophys. Res. Lett.*, *27*, 3237–3240.
- McIlwain, C. E. (1974), Substorm injection boundaries, in *Magnetospheric Physics*, edited by B. M. McCormac, pp. 143–154, D. Reidel, Dordrecht, Netherlands.
- Miyashita, Y., et al. (2009), A state-of-the-art picture of substorm-associated evolution of the near-Earth magnetotail obtained from superposed epoch analysis, *J. Geophys. Res.*, *114*, A01211, doi:10.1029/2008JA013225.
- Nakamura, R., T. Oguti, T. Yamamoto, S. Kokubun, D. N. Baker, and R. D. Belian (1991), Aurora and energetic particle signatures during a substorm with multiple expansions, in *Magnetospheric Substorms, Geophys. Monogr. Ser.*, vol. 64, edited by J. R. Kan et al., pp. 285–294, AGU, Washington, D. C.
- Nakamura, R., T. Oguti, T. Yamamoto, and S. Kokubun (1993), Equatorward and poleward expansion of the auroras during auroral substorms, *J. Geophys. Res.*, *98*, 5743–5759.
- Nishimura, Y., J. Wygant, T. Ono, M. Iizima, A. Kumamoto, D. Brautigam, and R. Friedel (2008), SAPS measurements around the magnetic equator by CRRES, *Geophys. Res. Lett.*, *35*, L10104, doi:10.1029/2008GL033970.
- Ohtani, S.-I. (1998), Earthward expansion of tail current disruption: Dual-satellite study, *J. Geophys. Res.*, *103*, 6815–6825.
- Rae, I. J., et al. (2009), Timing and localization of ionospheric signatures associated with substorm expansion phase onset, *J. Geophys. Res.*, *114*, A00C09, doi:10.1029/2008JA013559.
- Reeves, G. D., M. G. Henderson, P. S. McLachlan, R. D. Belian, R. H. W. Friedel, and A. Korth (1996), Radial propagation of substorm injections, paper presented at Third International Conference on Substorms, Versailles, France, 12–17 May.
- Runov, A., V. Angelopoulos, N. Ganushkina, R. Nakamura, J. McFadden, D. Larson, I. Dandouras, K.-H. Glassmeier, and C. Carr (2008), Multi-point observations of the inner boundary of the plasma sheet during geomagnetic disturbances, *Geophys. Res. Lett.*, *35*, L17S23, doi:10.1029/2008GL033982.
- Russell, C. T., and R. L. McPherron (1973), The magnetotail and substorms, *Space Sci. Rev.*, *15*, 205–265.
- Sergeev, V. A., and M. V. Kubyshkina (1996), Low altitude image of particle acceleration and magnetospheric reconfiguration at substorm onset, *J. Geomagn. Geoelectr.*, *48*, 877–885.
- Sergeev, V. A., et al. (2000), Multiple-spacecraft observation of a narrow transient plasma jet in the Earth's plasma sheet, *Geophys. Res. Lett.*, *27*, 851–854.
- Sergeev, V. A., S. V. Apatenkov, V. Angelopoulos, J. P. McFadden, D. Larson, J. W. Bonnell, M. Kuznetsova, N. Partamies, and F. Honary (2008), Simultaneous THEMIS observations in the near-tail portion of the inner and outer plasma sheet flux tubes at substorm onset, *J. Geophys. Res.*, *113*, A00C02, doi:10.1029/2008JA013527.
- Shukhtina, M. A., N. P. Dmitrieva, N. G. Popova, V. A. Sergeev, A. G. Yahnin, and I. V. Despirak (2005), Observational evidence of the loading-unloading substorm scheme, *Geophys. Res. Lett.*, *32*, L17107, doi:10.1029/2005GL023779.
- Torr, M. R., et al. (1995), A far ultraviolet imager for the international solar-terrestrial physics mission, *Space Sci. Rev.*, *71*, 329–383.
- Yahnin, A. G., I. V. Despirak, A. A. Lubchich, B. V. Kozelov, N. P. Dmitrieva, M. A. Shukhtina, and H. K. Biernat (2006), Relationship between substorm auroras and processes in the near-Earth magnetotail, *Space Sci. Rev.*, *122*, 97–106, doi:10.1007/s11214-006-5884-4.
- Zesta, E., L. Lyons, C.-P. Wang, E. Donovan, H. Frey, and T. Nagai (2006), Auroral poleward boundary intensifications (PBI): Their two-dimensional structure and associated dynamics in the plasma sheet, *J. Geophys. Res.*, *111*, A05201, doi:10.1029/2004JA010640.

V. Angelopoulos, Institute of Geophysics and Planetary Physics, University of California, Los Angeles, CA 90095, USA.

M. Fillingim, D. Larson, and J. P. McFadden, Space Science Laboratory, University of California, 7 Gauss Way, Berkeley, CA 94720, USA.

I. A. Kornilov and T. A. Kornilova, Polar Geophysical Institute, Russian Academy of Sciences, Murmansk Region, Apatity 184200, Russia.

M. V. Kubyshkina and V. A. Sergeev, Institute of Physics, St. Petersburg State University, Ulyanovskaya 1, Petrodvorets, Saint Petersburg 198504, Russia. (victor@geo.phys.spbu.ru)

R. Nakamura, Space Research Institute, Austrian Academy of Sciences, Schmiedlstr. 6, A-8042 Graz, Austria.